Understanding of gas-phase methane pyrolysis towards hydrogen and solid carbon with detailed kinetic simulations and experiments

Manas Mokashi [a], Akash Bhimrao Shirsath [a], Patrick Lott [a], Heinz Müller [a], Steffen Tischer [b], Lubow Maier [b], Olaf Deutschmann [a,b,*]

[a] Institute for Chemical Technology and Polymer Chemistry (ITCP), Karlsruhe Institute of Technology (KIT), D-76131 Karlsruhe, Germany
[b] Institute of Catalysis Research and Technology (IKFT), Karlsruhe Institute of Technology (KIT), D-76344 Eggenstein-Leopoldshafen, Germany

Keywords:
High temperature kinetics
Gas-phase methane pyrolysis
Hydrogen production
Light hydrocarbons
Empty tube reactor
Carbon coupling reactions

A B S T R A C T

Methane (CH_4) pyrolysis is studied in a tubular flow reactor for the production of hydrogen and solid carbon by combining kinetic modelling, numerical simulation and experiments in a high-temperature flow reactor. Operating conditions are varied such as temperature in the range of 1273–1873 K, hydrogen addition to the feed with a molar H_2:CH_4 ratio between 0 and 4, and residence time in the range of 3–7 s. Elementary-step reaction mechanisms consisting of pyrolysis and carbon coupling reactions among C_1, C_2, aromatic and polycyclic aromatic hydrocarbon species are used in the numerical simulations of the species profiles in flow direction. A thermodynamic analysis is performed to acquire the boundary conditions for operation as well to estimate probable by-products (C_2H_2, C_2H_4, C_2H_6, C_6H_6, $C_{16}H_{10}$ etc.) over the temperature range. Gas-phase kinetic modelling is performed revealing that CH_4 conversion starts at temperatures above 1273 K. Higher temperatures increase CH_4 conversion and H_2 yield peaking at 1573 K. The cooling temperature gradient downstream of the hot zone in the reactor causes reverse reactions in gas-phase suppressing CH_4 conversion. H_2 addition to the feed is found to be a crucial parameter for controlling the by-product formation. In the experimental study, a solid carbon yield of 84 % is achieved while gaseous by-products remain less than 1 mol-% at 1673 K, H_2:CH_4 ratio of 2, and residence time of 5 s. Gas-phase reactions are found to be coupled to surface reactions at higher temperatures.

1. Introduction

Hydrogen (H_2) is expected to play an important role as a modern carbon-free energy carrier that allows for substantial reduction of global greenhouse gas emissions [1–3]. H_2 is also one of the most important basic chemicals used for the production of ammonia, during petroleum refining, and for methanol synthesis [4]. Therefore, it is of great interest to develop a H_2 production process that is environmentally friendly, economically competitive and suitable for large-scale industrial application.

Presently, multiple state-of-the-art catalytic technologies are available for H_2 production from natural gas. Steam methane reforming (SMR) is well-established for H_2 and simultaneous carbon monoxide (CO) production as it is a cost-effective path [1,5,6]. However, it releases significant quantities of carbon dioxide (CO_2) as a by-product and requires additional carbon capture and storage processes [7–9]. Additionally, catalytic partial oxidation of methane (CPOX) [10–12], autothermal reforming of methane (ATR) [13] and dry reforming of methane (DRM) [14–16] are also commercially viable processes used to produce H_2 for different applications. Nevertheless, all these processes produce synthesis gas, a mixture of H_2 and CO along with CO_2, as a by-product and not pure H_2. Environmentally friendly H_2 can be produced with water electrolysis using renewable energy [17]. However, water electrolysis has a very high energy demand which is a bottleneck [18]. Furthermore, the use of H_2 as energy carrier stored in metals and metal hydrides via oxidation–reduction cycles has also been getting attention recently [19–21].

Methane (CH_4) pyrolysis according to Equation (1) is not only a process that does not produce direct CO_2 emissions, but also offers the chance to extract carbon from gaseous methane, e.g. from natural gas, making it a bridging technology towards a sustainable energy supply. Furthermore, the use of biomethane originating from biomass gasification as feedstock for pyrolysis is a promising technology to remove carbon from the atmosphere that can either be sequestrated or used in

* Corresponding author at: Bldg. 11.21, KIT-Campus South, Engesserstr. 20, 76131 Karlsruhe, Germany.
E-mail address: deutschmann@kit.edu (O. Deutschmann).

further processes. Rather than a mere sequestration, the further usage of accruing solid carbon improves the economic viability even further [1,8,22].

$$CH_{4\ (g)} \rightarrow C_{(s)} + 2H_{2\ (g)}\ \Delta H_R^0 = +76\text{kJ mol}^{-1} \quad (1)$$

In order to maximize methane conversion and product selectivity, various metal and carbon catalysts as well as the role of promoters and supports have been widely studied and reviewed in literature [2,9,23,24]. In addition, different reactor concepts such as molten metal bubble column reactors [25], thin film reactors [26], and plasma reactors [27,28] were suggested in order to realize an efficient overall process. Aside from thermal activation, plasma methane pyrolysis has also been investigated [29–31]. More recently, Magazova et al. [32] and Kreuznacht et al. [33] investigated plasma methane pyrolysis on the laboratory scale. A maximum CH_4 conversion of 65 % was achieved using an argon-diluted feed containing 1 vol-% CH_4 [33].

In our previous work we studied the feasibility of thermal CH_4 pyrolysis at industrially relevant conditions achieving CH_4 conversions up to 99 % and H_2 yields near 100 %, respectively, at 1873 K, 1 bar, a residence time of 1 s, and a H_2:CH_4 molar feed ratio of 4 [34]. In addition, a beneficial effect of solid carbon was revealed by introducing a carbon foil or mesh in the reactor [34].

The CH_4 pyrolysis reaction progresses via carbon coupling reactions [35–43], leading to the formation of light hydrocarbons, aromatic hydrocarbons and polycyclic aromatic hydrocarbons in sequence as:

$$CH_4 \rightarrow C_2H_6 \rightarrow C_2H_4 \rightarrow C_2H_2 \rightarrow C_6H_6 \rightarrow \text{Pyrene} \quad (2)$$

Most of the literature suggests a free radical reaction sequence with CH_3 radical formation as the first initiation step [18,35,39,44,45]. The initial reaction mechanism leading up to C_3 species was proposed by Chen et al. [35] and later extended by Roscoe and Thompson [36] by adding reverse reactions, isomerization reactions, and additional C_3 products. However, the Roscoe-Thompson [36] mechanism was developed for temperatures only up to 1100 K. Dean [37] studied CH_4 pyrolysis kinetics at low temperature (1038 K) and pressure (0.58 bar) and further extended the mechanism until the formation of a benzene (C_6H_6) ring. Flow reactor studies were performed by Billaud et al. [38] at 1453–1503 K, 1 bar and residence time up to 0.2 to 1.5 s, while Holmen et al. [39] performed mechanistic studies up to 1573 K at short residence times up to 0.4 s and a pressure of 0.13 bar. The focus of the studies by Billaud et al. [38] and Holmen et al. [39] was on C_2 species formation and not H_2 production, hence, the process conditions were also selected accordingly. Hidaka et al. [40] developed a detailed mechanism for a broad temperature range of 1350–2400 K and pressure of 1.6 to 4.4 bar to model shock tube experiments. The mechanism considers reactions of hydrocarbon species up to C_6H_6 formation. Appel et al. [41] developed a detailed C_1 and C_2 mechanism including both combustion and pyrolysis reaction sets. Importantly, the mechanism also considers the formation of polycyclic aromatic hydrocarbons (PAHs) up to pyrene. Their simulation studies also focused on shock tube experiments in the context of combustion. Sinaki et al. [46] updated the mechanism by Appel et al. [41] by replacing 19 rate coefficients from the available literature mechanisms from the NIST kinetic database [47] and found a good agreement between their model and pyrolysis experiments by Back et al. [48], Shah et al. [49], and Murphy et al. [50] for temperatures of up to 1450 K. The pyrolysis mechanisms of light hydrocarbons, including ethylene (C_2H_4), acetylene (C_2H_2), and propylene (C_3H_6), have also been explored with the primary focus on synthesis of carbon–carbon composites [42,51,52].

However, none of the above-mentioned kinetic studies focused on CH_4 pyrolysis with the objective of formation of solid carbon aside from hydrogen formation. In the current work, a combined numerical simulation and experimental study is performed for homogeneous gas-phase pyrolysis of methane-hydrogen mixtures at high temperature. The simulations are compared with end-of-pipe measurements conducted in a flow reactor for model evaluation. Furthermore, axial profiles of hydrocarbon species along the flow direction are analyzed to gain a deeper understanding of the gas-phase chemistry involved in CH_4 pyrolysis.

2. Experimental

Experiments were conducted in a tubular flow reactor designed for kinetic studies at high temperature (up to 2073 K) and elevated pressure (up to 10 bar) as previously described by Angeli et al. [53]. The reactor consists of a ceramic α-Al_2O_3 tubular reactor of 1 m length and of 2 cm inner diameter, in which heating elements and insulation create an isothermal hot zone of 0.4 m. The reaction gas mixture was fed via mass flow controllers and the mixture was preheated to 443 K. The operating conditions were controlled by a LabView-based software tool and the effluent (product) gas stream was continuously analyzed with an online HPR-20 mass spectrometer (Hiden Analytical), focusing on quantification of H_2, CH_4, C_2H_2, C_2H_4, C_2H_6, and C_6H_6. During the measurement campaign, temperature, feed molar ratio of H_2:CH_4, and the residence time were varied to study their influence on methane conversion and product selectivity. The operating conditions studied are summarized in Table 1. In analogy to a previous publication from our group [54], the sum of the experimental error bars with regard to gas-phase species quantification and carbon balance is less than 5 %.

3. Modeling approach

3.1. Flow reactor model

The reactor was simulated using a one-dimensional (in flow direction) plug flow reactor model. Assuming steady state and non-dispersive flow conditions, the model is developed based on a continuum modeling approach. The present model solves the species mass balance as shown in Equation (3).

$$\rho u \frac{dY_i}{dz} = M_i \dot{\omega}_i, \quad (3)$$

where M_i is the molar mass of species i, ρ is the gas-phase density, u is the gas velocity, z is the axial coordinate, $\dot{\omega}_i$ is the rate of formation of gas-phase species i, and Y_i is the mass fraction of species i.

$$\dot{\omega}_i = \frac{dc_i}{dt} = \sum_{k \in R_g} (\nu''_{ik} - \nu'_{ik}) k_k \prod_{j \in S_g} c_j^{\nu'_{jk}} \quad (4)$$

where, ν'_{ik} and ν''_{ik} are the stoichiometric coefficients of the forward and reverse reactions, respectively, c is the concentration in gas-phase, k_k is the rate constant of reaction k and S_g is the set of gas-phase species.

Furthermore, the present model computes residence time based on the Equation (5) shown below.

$$\frac{d\tau}{dz} = \frac{1}{u}, \quad (5)$$

where τ is the residence time. The actual temperature profile measured along the reactor's axial direction is included into the simulations to give the local temperature. The computer code DETCHEM^{PFR} is used for the numerical simulations [55–58].

Table 1
Process conditions varied in the experiments.

Process parameter	Variation range
Temperature	1273–1473–1673–1873 K
H_2:CH_4 molar feed ratio	1–2–4
Residence time	3–5–7 s
Pressure	1 bar

3.2. Reaction flow analysis

Analogous to the methodology described in the work of Gossler et al. [59], the contribution of the specific reaction to the formation or consumption of species is analyzed with the help of a reaction flow analysis (RFA), also known as reaction path analysis.

The computer code DETCHEM^{PFR} computes the rate for each reaction at any axial position in the reactor. Both local and integral reaction flow analysis can be performed. The local rate of reaction r_k of the k-th reaction given by Equation (6),

$$r_k = k_{fk}\prod_{i\in S_g} c_i^{\nu'_{jk}} \quad k_{rk}\prod_{i\in S_g} c_i^{\nu''_{jk}}, \tag{6}$$

where k_{fk} is the rate of forward reaction, k_{rk} is the rate of reverse reaction and c_i is the concentration of species i in gas-phase. To determine the contribution $\dot{n}_{ik}$ of a reaction k to the production species i the rate of reaction r_k must be multiplied by the effective stoichiometric coefficients (ν''_{ik} ν'_{ik}) resulting in a matrix with the dimension of total species by total reactions. The data is then normalized by dividing the values of the contributing species by the sum of those values. This is done separately for the formation (Equation (7)) and consumption (Equation (8)) of each species,

$$\dot{n}^{\text{form}}_{\text{normalized, }ik} = \frac{\dot{n}^{\text{form}}_{ik}}{\sum_{k\in R_g}\dot{n}^{\text{form}}_{ik}} \tag{7}$$

$$\dot{n}^{\text{cons}}_{\text{normalized, }ik} = \frac{\dot{n}^{\text{cons}}_{ik}}{\sum_{k\in R_g}\dot{n}^{\text{cons}}_{ik}} \tag{8}$$

where R_g is the set of gas-phase reactions.

An analogous approach is employed for integral reaction flow analysis, where the local rates r_k are replaced by total rates of production R_k

$$R_k = \int_0^t r_k dt, \tag{9}$$

where t is the time.

In the software used, the integration can also be stopped at a specified residence time or axial position in the reactor.

3.3. Reaction mechanisms

For the interpretation of experimental data and further development of the process, a reliable and detailed kinetic mechanism is vital. Detailed kinetic mechanisms by Appel et al. [41] (hereinafter referred to as ABF2000), Golovitchev et al. [60] (Golov1999), Norinaga and Deutschmann [52] (ND2007), and Porras et al. [43] (PolyMech) were reviewed in this study.

ABF2000 was originally developed for the combustion of light hydrocarbons. Nevertheless, the mechanism also comprises the pyrolysis of C_1 and C_2 species along with carbon coupling reactions. Reactions of small hydrocarbons in ABF2000 were taken from the previously published GRI-Mech 1.2 [61]. Herein, the formation of benzene (C_6H_6) by coupling reactions is described by three pathways: The propargyl radical path, the C_4H_x path and a C_6H_x path involving cyclization reactions. Furthermore, the formation of polycyclic aromatic hydrocarbons (PAHs) until pyrene takes place via H-abstraction and C_2H_2-addition, which is commonly known as the so-called HACA reaction sequence. Since the original ABF2000 mechanism also comprises combustion reactions, it was first adapted to pyrolytic conditions by removing all oxygen-related species and reactions, which reduces the mechanism to 76 species and 247 reactions. Herein, the propargyl recombination reaction has a critical role in benzene formation as discussed in detail in section 4.3. The ABF2000 mechanism defines this reaction as an irreversible reaction leading to thermodynamic inconsistency at temperatures above 1673 K, therefore it was replaced by a reversible reaction from PolyMech.

Similar to ABF2000, also Golov1999 was adapted to pyrolytic conditions since it was originally developed for describing the combustion of various hydrocarbon-based fuels. After adaption, it comprises 84 species and 236 reactions. The Golov1999 mechanism includes reaction paths leading up to the formation of the C_6H_6 ring and a series of irreversible reactions for anthracene production, which is regarded as an inception molecule for soot. Moreover, C_4H_2 is also considered a soot precursor in this mechanism.

PolyMech was originally developed for dimethyl-ether and methane combustion, but also includes a sub-mechanism of C_1 pyrolysis reactions. It is based on the work by Hidaka et al. [40] on CH_4 oxidation and pyrolysis. It was reduced to 44 species and 143 reactions that exclusively consider the CH_4 pyrolysis process. Hence, PolyMech is the smallest reaction mechanism among all the mechanisms discussed herein, resulting in the lowest computational expenses. However, it considers coupling reactions only until C_6H_6 formation and no further formation of PAHs is taken into account.

ND2007 was developed for describing the pyrolysis of ethylene, acetylene, and propylene and involves not only reactions for C_1 pyrolysis but also comprises C_3 pathways, resulting in a comprehensive mechanism with 227 species and 827 reactions. While parts of the ND2007 mechanism have their origin in the ABF2000 mechanism, ND2007 also includes odd carbon number PAHs and is extended up to coronene formation.

All the aforementioned mechanisms are valid over a large range of conditions well within the scope of this study, however, all have certain advantages and limitations. In the following, ABF2000 and PolyMech are considered for detailed studies due to detailed C-C coupling reactions as well as smaller sizes. All the mechanisms are provided in the supporting information.

4. Results and discussion

4.1. Thermodynamic analysis

Along with H_2 and carbon production, CH_4 pyrolysis produces various hydrocarbon species as intermediates. Therefore, a comprehensive thermodynamic analysis of the reacting system was performed to investigate equilibrium boundaries associated with CH_4 pyrolysis.

For the present study, thermodynamic calculations were performed using the DETCHEM software package [55] along with the HSC Chemistry Software [62]. DETCHEM^{EQUIL} was applied to calculate equilibrium compositions for a specified feed gas mixture under constant pressure and isothermal conditions. On the other hand, HSC Chemistry was used to calculate the change in the Gibbs energy of reaction ($\Delta_r G$) for a given temperature range.

A negative $\Delta_r G$ is required for a thermodynamically feasible reaction. Fig. 1 shows the $\Delta_r G$ values for various carbon coupling reactions from CH_4 for a wide temperature range. In general, CH_4 pyrolysis is thermodynamically viable for temperatures higher than 800 K. For temperatures greater than 1373 K, the formation of aromatics and PAHs is also feasible, and for temperatures higher than 1573 K, also direct carbon coupling reactions to light hydrocarbons such as C_2H_2 and C_2H_4 become possible. However, the methane pyrolysis reaction remains thermodynamically most favorable for the entire temperature range shown, i.e., 773–2273 K.

The equilibrium product distribution is another important facet that is necessary to understand equilibrium limitations under specified process conditions. Fig. 2 (a) shows the equilibrium product distribution considering gas-phase species present in the adapted ABF2000 mechanism. The molar ratio of H_2:CH_4 is defined as 2, the pressure is set to 1 bar, and the temperature is varied between 773 K and 2273 K. The data depicted in Fig. 2 (a) underscore that the equilibrium shifts towards H_2 at higher temperatures, showing a peak at around 1600 K. C_2H_2 is the most dominant by-product, reaching a mole fraction of 0.1 for

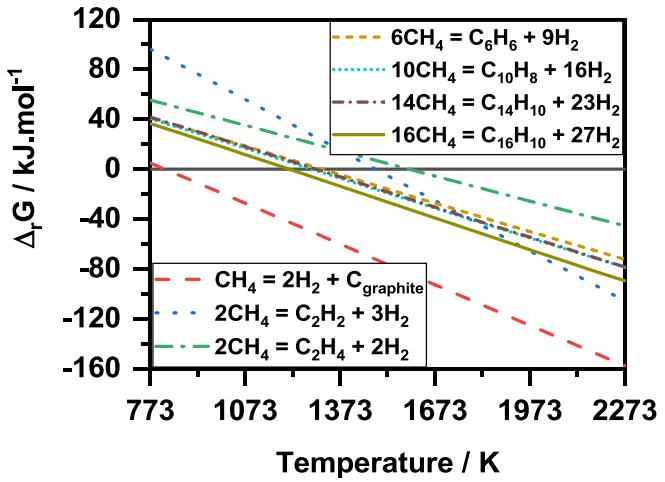

Fig. 1. Gibbs energy of reaction ($\Delta_r G$) for carbon coupling reactions from methane over a temperature range.

temperatures above 1773 K. Other by-products such as $C_{16}H_{10}$ (pyrene), C_2H_4, and C_6H_6 are also formed reaching peak values around 1623 K, but quickly disappear with rising temperature. By incorporating graphite as an additional species in the calculations, a significant shift in the equilibrium towards H_2 is observed at lower temperature of 873 K. Additionally, by-product formation is also significantly suppressed (Fig. 2 (b)).

Moreover, the impact of pressure on the equilibrium product distribution was examined. While keeping the molar ratio of H_2:CH_4 constant to 2, the equilibrium product distribution was simulated at three different pressures: 1, 5, and 10 bar. The simulations revealed a declining H_2 mole fraction with rising pressure, which is most pronounced between 1173 K and 1973 K, whereas the pressure plays a negligible role for temperatures higher than 1973 K (Fig. 3 (a)). Furthermore, increase in pressure suppresses the formation of by-products. As shown in Fig. 3 (b), the pyrene peak mole fraction is reduced with increasing pressure and additionally, the peak position is shifted towards higher temperatures. A similar trend as for the main by-product C_2H_2 is also observed for pyrene (Fig. S1).

In summary, the thermodynamic analysis shows that CH_4 pyrolysis is thermodynamically favored for temperatures higher than 1073 K and the presence of graphitic carbon facilitates a further shift of the equilibrium towards H_2. In addition, increasing pressure has a negative effect on the formation of H_2.

4.2. *Comparison of experiments with simulations*

In this section, numerical simulations are compared to the experimental measurements. Experimentally varied process conditions are shown in Table 1. The experimental reactor (1.0 m) exhibits a preheating zone (0.35 m) located upstream of the hot zone (0.4 m) and a downstream cooling zone (0.25 m). While the hot zone can be operated under isothermal conditions, the temperature is rising and declining in the zones up- and downstream, respectively. Using argon (Ar) as flowing medium, two axial temperature profiles were measured in the experimental setup, choosing either 1473 K or 1673 K as set-points for the heating element control. Although the heat capacity of the reaction gas mixture differs from that of Ar, only a minor impact on the temperature profiles is expected. Since the simulations cover a much wider range of setup operation conditions, the experimentally obtained temperature profiles were extrapolated or interpolated as shown in Fig. 4. These temperature profiles were then used as inputs for the reactor simulations.

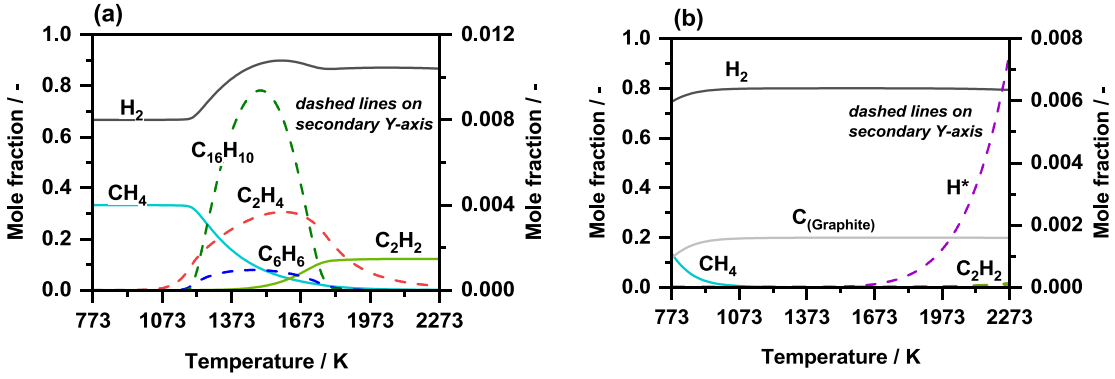

Fig. 2. Equilibrium product distribution for a molar ratio of H_2:CH_4 of 2; (a) only gas-phase species and (b) gas-phase species plus graphitic carbon.

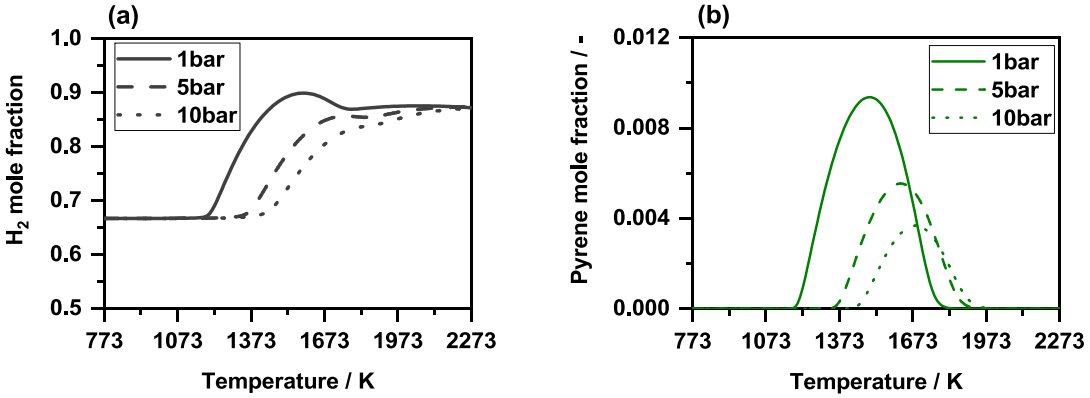

Fig. 3. Impact of pressure on equilibrium distribution (a) hydrogen formation and (b) Pyrene formation.

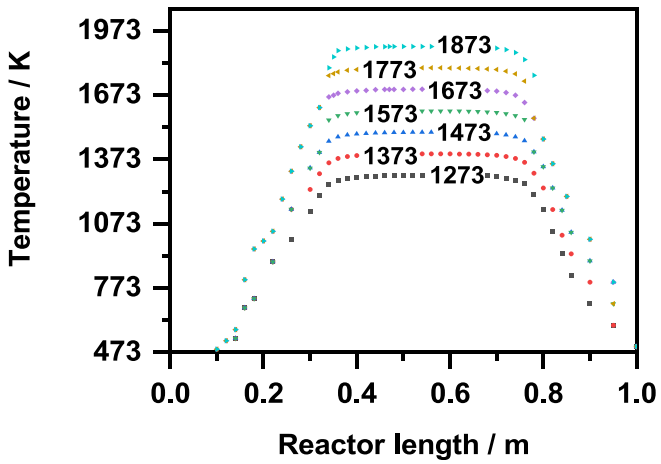

Fig. 4. Experimentally measured axial temperature profiles for 1473 K and 1673 K. Numerically inter- and extrapolated temperature profiles for 1273, 1373, 1573, 1773 and 1873 K.

4.2.1. Impact of temperature

CH_4 is a stable molecule and therefore the pyrolysis reaction requires very high temperatures. This section explains the effect of temperature on CH_4 pyrolysis and lays a particular focus on the temperature regime between 1273 K and 1873 K, which is considered feasible for industrial applications. Herein, the H_2:CH_4 molar feed ratio of 2, residence time of 5 s, and pressure of 1 bar is kept constant.

Fig. 5 shows the experimentally determined composition of the effluent gas stream in comparison with the ABF2000 and PolyMech simulations. For temperatures up to 1473 K, the simulations are in good agreement with experiments regarding CH_4 and H_2 mole fractions (Fig. 5 (a)). For temperatures higher than 1673 K, however, simulations and experiments show a higher deviation. At 1273 K, CH_4 conversion in the experiment is as low as 19 %, with only very low by-product levels. Upon increasing the temperature, from 1373 K onwards both CH_4 conversion as well as the formation of by-products increase rapidly, reaching 65 % CH_4 conversion at 1473 K and 90 % at 1673 K (Fig. S2). Above 1673 K, the CH_4 conversion slightly decreases. Based on Fig. 2 (a), it is clear that the process is limited by equilibrium. Among the by-products in the experiments, C_2H_4 is detected as the most prominent by-product, followed by C_6H_6 (Fig. 5 (b)). However, above 1673 K C_6H_6 does not survive and C_2H_4 steadily decrease. Compared to the experimental data, ABF2000 overpredicts the formation of C_2H_4 while PolyMech overpredicts the formation of C_6H_6.

Along with the end-of-pipe analysis, axial profiles also contain important information on the reaction progress. They are particularly important in this study, since the temperature varies along the reactor length. Fig. 6 (a) shows the axial profiles for the main species H_2 and CH_4, while Fig. 6 (b) shows the development of by-products for both mechanisms, ABF2000 and PolyMech at 1673 K. Both mechanisms yield very similar profiles for the main species. CH_4 and H_2 mole fractions almost reach a plateau around a reactor length of 0.5 m. However, after the hot zone (reactor length 0.75 m), the CH_4 mole fraction climbs up and in the same region, the H_2 mole fraction goes down suggesting it is consumed. Among the by-products, both the mechanisms predict C_2H_2 as major species, reaching more than 8 mol-% in the hot zone of the reactor. In case of ABF2000, the slow decrease in C_2H_2 after a reactor length of 0.4 m is attributed to its consumption via HACA reaction sequence to form PAHs, whereas in PolyMech, it remains constant until 0.75 m of reactor length. C_2H_4 and C_6H_6 are also estimated in small quantities, but the trends are different in both mechanisms. As the cooling zone begins around 0.75 m from the reactor length, C_2H_2 rapidly drops down while C_2H_4 and C_6H_6 rise. A detailed explanation regarding these trends is presented in section 4.3. Fig. 6 (c) illustrates the axial profiles of the main products at 1473 K. Similar to the findings for 1673 K, H_2 formation starts at approx. 0.3 m downstream of the reactor inlet at 1473 K. However, the lower temperature results in a longer reaction zone that is required for CH_4 conversion and H_2 production. Nonetheless, differences of the CH_4 levels at the reactor outlet are marginal at the reactor outlet as the jump in CH_4 mole fraction around 0.75 m is smaller in case of 1473 K. Fig. 6 (d) depicts the simulated axially resolved by-product formation along the reactor length at 1473 K. Compared to 1673 K, considerably less C_2H_2 formation but more C_6H_6 formation is observed at 1473 K. The C_2H_4 trend is relatively similar for both temperatures. For temperatures 1273 K (Fig. S3 (a) and (b)) and 1873 K (Fig. S3 (c) and (d)) axial profiles are provided in the supplementary information.

In general, the simulations with both mechanisms agree well with our experimental results regarding CH_4 and H_2 concentrations up to 1473 K. However, for temperatures above 1673 K the simulations are underpredicting CH_4 consumption. Carbon formation on the reactor wall and in the filters downstream of the reactor are observed in the experiments as reported in our previous experimental study [34]. This formation of solid carbon and soot particles implies that the high-temperature decomposition of gas-phase CH_4 is not only taking place in the gas-phase, but also comprises heterogeneous reaction paths. Several hydrocarbon by-products can contribute to solid carbon formation, either via a soot formation mechanism or by surface deposition. The important role of C_2H_2 in soot formation and carbon deposition at higher temperatures has been subject to numerous studies [52,63–66]. It is consensus that during soot formation C_2H_2 is consumed by the HACA sequence to form PAHs while releasing H_2 [41,67]. Similarly, various light hydrocarbons can release H_2 molecules when forming a carbon deposited layer on a surface [66,68–72]. The axial profiles in Fig. 6 (b) also support the important role of C_2H_2, even though it does not survive

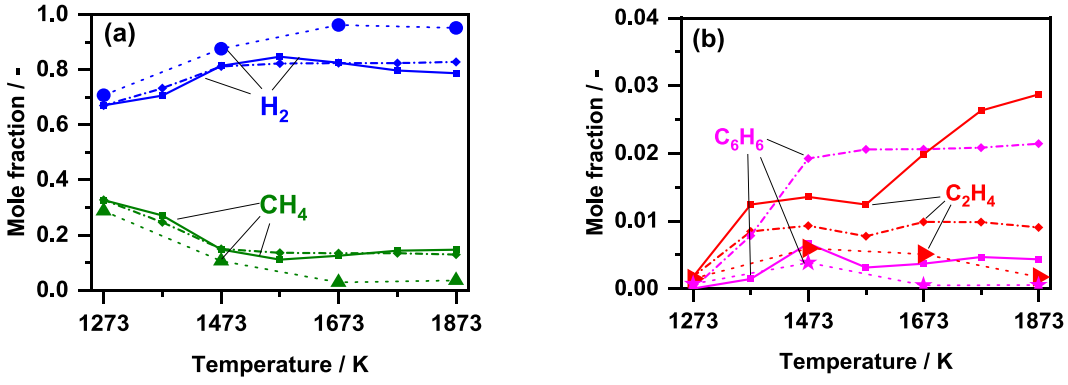

Fig. 5. Full reactor simulated and experimental end-of-pipe profiles vs. temperature; (a) main products, (b) by-products (solid line with (■): ABF2000 simulations, dot-dashed line with (◆): PolyMech simulations while dotted line with (●), (▲), (►) and (★) denotes measured mole fractions).

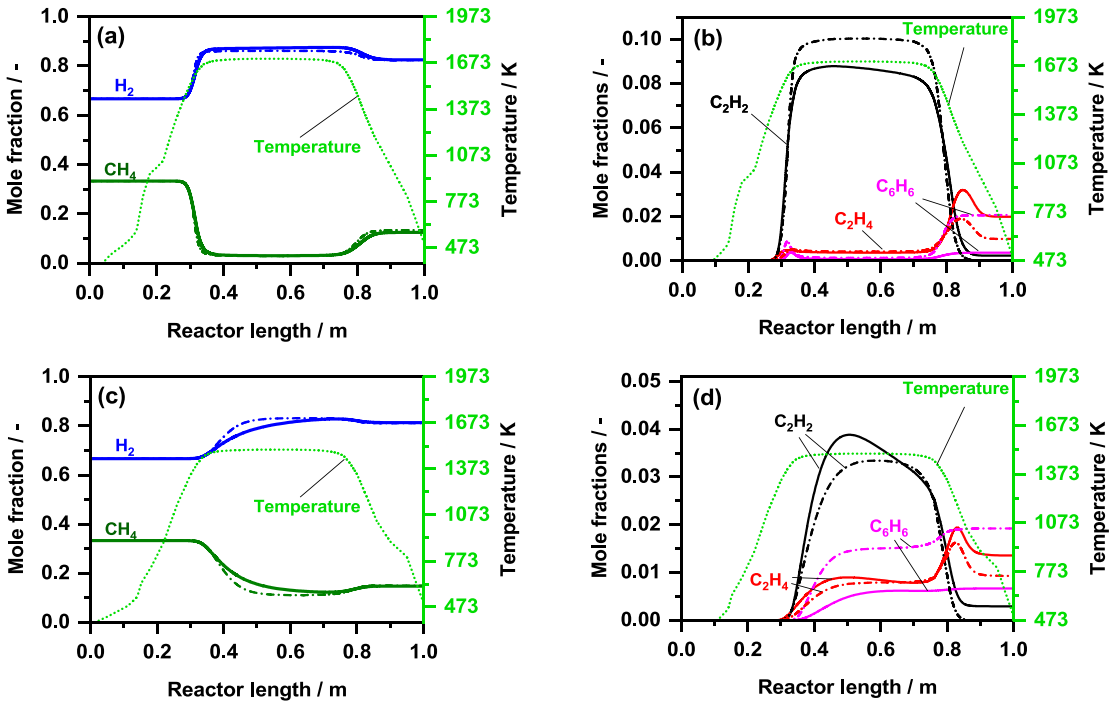

Fig. 6. Axial profiles describing ABF2000 and PolyMech simulations of a full reactor with temperature profiles. (a) Consumption of reactant CH_4 along with the H_2 evolution at hot zone temperature of 1673 K, (b) development of by-products at hot zone temperature of 1673 K, (c) consumption of reactant CH_4 along with the H_2 evolution at hot zone temperature of 1473 K and (d) development of by-products at hot zone temperature of 1473 K; conditions: 1 bar, H_2:CH_4 molar ratio of 2, residence time of 5 s; solid line for ABF2000, dot-dashed line for PolyMech.

to the end of the reactor. Furthermore, the formation of solid carbon through heterogeneous reactions allows the gas-phase equilibrium limit to be crossed in experiments, resulting in more H_2 production. Compared to experiments, simulations produce less H_2 and can be correlated to the absence of a surface mechanism. To fully understand and optimize CH_4 pyrolysis, it is essential to investigate interactions between gas-phase and surface mechanisms. In the current model, PolyMech is limited in its capabilities, only including reactions up to C_6H_6 and not being able to couple soot formation mechanisms. On the other hand, ABF2000 includes PAHs formation up to pyrene. Therefore, it is more suitable to gain a comprehensive understanding of gas-phase, soot and deposition interactions. Consequently, in-depth studies of ABF2000 are performed and compared to experimental results in the next chapters.

4.2.2. *Impact of hydrogen content in feed*

Since previous research points to an inhibition of CH_4 pyrolysis by hydrogen [39,64,73], this section investigates the impact of the hydrogen content (H_2:CH_4 molar ratio) in the feed gas on the CH_4 pyrolysis reaction. Notably, the presence of H_2 can inhibit both homogeneous gas-phase reactions as well as heterogeneous surface deposition [64]. The gas-phase inhibition may be explained by the reverse direction of Equation (10).

$$CH_4 + H \rightleftharpoons CH_3 + H_2 \tag{10}$$

As the reaction is considered to be in equilibrium, the presence of H_2 converts methyl radicals into CH_4, thus reducing the CH_4 conversion [73]. Holmen et al. [73] reported a decrease in CH_4 conversion of about 20 % when the feed H_2:CH_4 molar ratio was increased from 1 to 4 at 1573 K, which is a significant impact. However, Holmen et al. [73] considered only residence times lower than 0.4 s, whereas the current work focuses on the impact the of H_2:CH_4 molar ratio in the feed for a residence time of 5 s, a temperature range of 1273–1873 K, and a pressure of 1 bar.

Fig. 7 (a) shows end-of-pipe experimental and ABF2000 full reactor simulation results at varying H_2:CH_4 molar ratios and temperatures. For less severe conditions, i.e. up to temperatures of 1473 K and higher dilution of 4, the simulations agree well with the experiments. In order to study the overall impact in detail, Fig. 7 (b) shows CH_4 conversion and H_2 yield in simulations for 1373 K and 1573 K, as at these temperatures intermediate and maximum levels of H_2 formation are observed. Increasing the H_2:CH_4 molar ratio from 0 to 4 in feed considerably reduces CH_4 conversion from 83 % to 46 % at 1573 K, while the H_2 yield is also halved. At 1373 K, an increase of the H_2:CH_4 molar ratio from 0 to 2 results in a reduction of both CH_4 conversion and H_2 yield. An increase of the ratio beyond a factor of 2 does not result in a further substantial suppression.

Furthermore, the results shown in Fig. 7 (c) and (d) reveal an impact of the H_2:CH_4 molar ratio on the simulated product carbon ('C') distribution. At 1373 K (Fig. 7 (c)), the majority of the carbon remains in unconverted CH_4, irrespective of the H_2 dilution. C_2 species account for 19 % of the carbon if no H_2 is added to the feed gas stream, which steadily decreases with increasing H_2 content. C_6 remains below 10 % while C in PAHs is negligible. For 1573 K, however, the C distribution is more diverse. C_{12} and C_{16} species account for more than 60 % of the total C while unconverted CH_4 is merely 17 % when choosing a CH_4-only feed. Increasing the H_2:CH_4 molar ratio to 4 results in a pronounced reduction of the PAHs share in C to only 12 %. On the other hand, the contribution of C_2 and C_6 hydrocarbons increases from 18 % to 32 % in the same range.

As already mentioned in the previous section, the experiments cross the equilibrium limit due to solid carbon formation at higher temperatures, which the current model cannot describe. However, for all H_2:CH_4 molar feed ratios, the ABF2000 mechanism agrees well with the experiments at lower temperatures, and follows the equilibrium curve at higher temperatures. Therefore, it is reasonable to assume that the ABF2000 mechanism captures gas-phase CH_4 pyrolysis reactions accurately also with respect to the increased H_2 content in the feed.

Overall, the H_2:CH_4 molar feed ratio is a key process parameter for controlling CH_4 conversion, H_2 yield, and C distribution in the (by-)

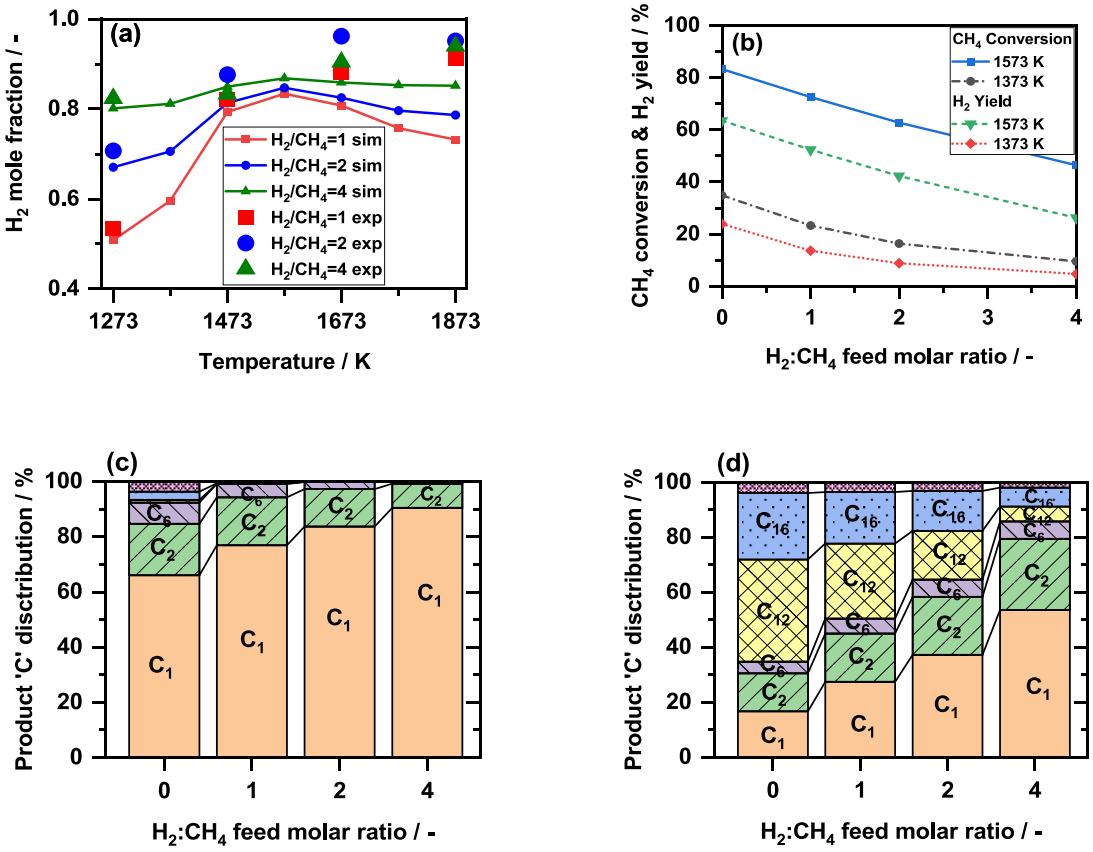

Fig. 7. Impact of H_2:CH_4 molar feed ratio in feed at a residence time of 5 s. (a) End-of-pipe experimental and simulation comparison for H_2:CH_4 variation and temperature variation; (b) impact of H_2:CH_4 variation on CH_4 conversion and H_2 yield in simulations; (c) Simulation 'C' distribution in product for 1373 K; (d) Simulation 'C' distribution in product for 1573 K (orange solid bar: C_1, green left side diagonal: C_2, violet right side diagonal: C_6, yellow cross: C_{12}, blue dots: C_{16}, pink small cross: remaining). (For interpretation of the references to colour in this figure legend, the reader is referred to the web version of this article.)

products. A higher H_2:CH_4 molar feed ratio results in a decrease in CH_4 conversion, but it also allows for a better control over soot formation by reducing the formation of PAHs.

4.2.3. *Impact of residence time*

Among the many factors that influence the CH_4 pyrolysis reaction, also the residence time (τ) in the hot zone is an important descriptor. Previously, Billaud et al. [38], Holmen et al. [39], and Olsvik et al. [73] studied the impact of τ on CH_4 pyrolysis. In these studies, the residence time τ was kept very small (<1.5 s) and a very high impact on the product distribution was reported. At 1673 K and H_2:CH_4 feed ratio of 2, when τ increased from 0.02 to 0.1 s, CH_4 conversion was increased by around 70 % and C_2 yield was raised by around 30 % [73]. For 1503 K and H_2:CH_4 feed ratio of 2, effect of τ was studied between 0.25 and 1.0 s [38]. CH_4 conversion was increased from 11 % to 41 % in the τ range but C_2 yield reached a peak of 20 % at 0.8 s which later slowly decreased [38]. It was also observed that coke formation increased with increase in τ [38]. For shorter residence times (<1 s) it is clear that the τ impacts greatly on CH_4 pyrolysis chemistry. However, the focus of these studies was on achieving high C_2 yields and not on obtaining high CH_4 conversions or H_2 yields. Considering potential industrially relevant residence times of 3 s to 7 s, this section shines a light on the impact of residence time on CH_4 conversion and H_2 yield.

Fig. 8 (a) compares end-of-pipe experimental data with full reactor simulations using the ABF2000 mechanism for τ and temperature variations. Overall, H_2 production is increased up on increasing the τ in experiments, however, for 5 s and 7 s error bars in the mass spectrometer data are too large to distinguish a clear difference. At higher temperatures (>1573 K) an influence of solid carbon similar to previous sections is also observed here. In simulations, CH_4 conversion and H_2 yield are not significantly affected by residence time variations between 3 and 7 s (Fig. 8 (b)). However, the simulations point to a clear impact of residence time on the formation of PAHs especially at 1573 K (Fig. 8 (c) and (d)). Even at 1373 K, and increase of τ from 3 s to 7 s results in an increase in C_6 share in the product composition as reactions move forward from light hydrocarbons to aromatics. For 1573 K this effect is intensified as the C_{14} + C_{16} share in the product composition increases substantially when τ is increased. This means that with respect to gas-phase reactions, the simulations suggest no advantage regarding CH_4 conversion and H_2 yield if the residence time is increased, but point to a promoted formation of PAHs. Soot formation via heterogeneous reactions can be related to the availability of PAHs, which means that an increasing residence time would also increase soot formation within the reactor. On the other hand, increasing the residence time even further would barely impact surface deposition reactions as these reactions are expected to be faster than the gas-phase reactions.

4.3. *Reaction flow analysis*

In the previous sections full-length reactor simulations are compared with the experimental data that were obtained in a plug-flow reactor that exhibits a pre-heating zone, a hot zone and a cooling zone. Especially the effect of the cooling zone on the axial species profiles depicted in Fig. 6 makes it necessary to study the reaction progress in more detail. In order to exclusively investigate the impact of temperature and to avoid other effects, isothermal simulations were performed with the computer code DETCHEM^{PFR} using two gas-phase mechanisms, ABF2000 and PolyMech, keeping H_2:CH_4 molar ratio in feed of 2, residence time of 5 s and pressure 1 bar. In addition, an integral reaction flow analysis (RFA) was conducted for both mechanisms to investigate

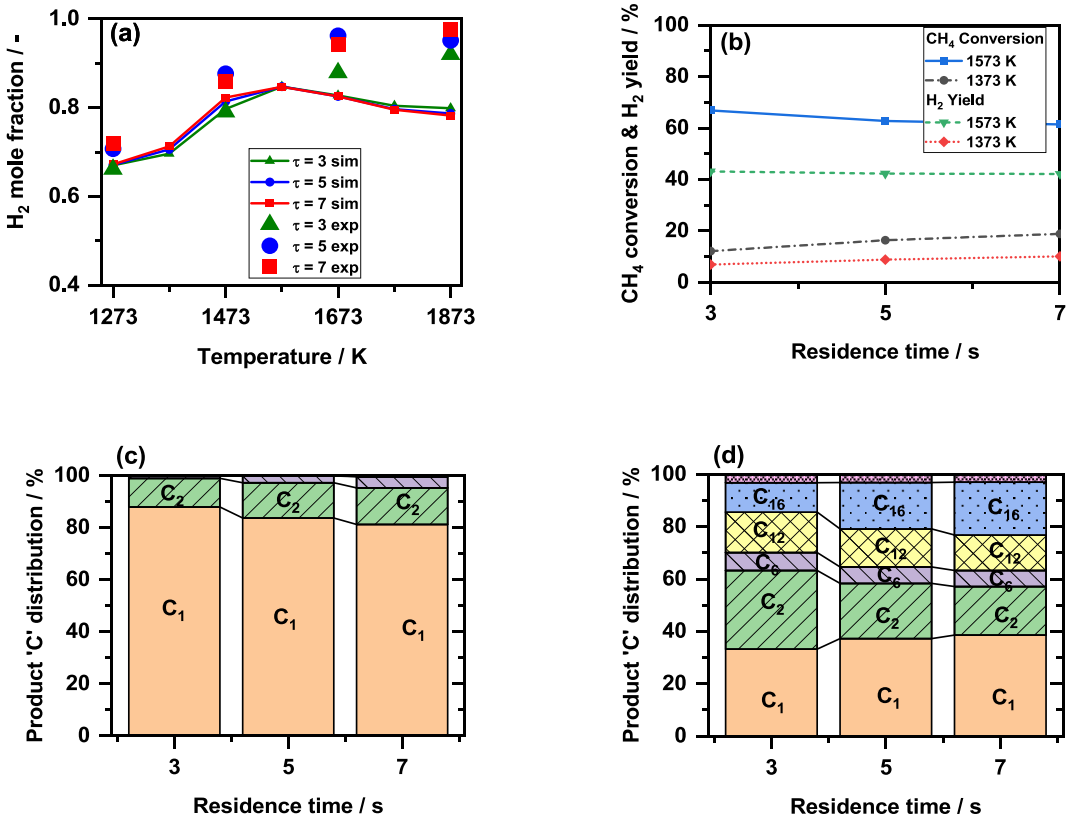

Fig. 8. Impact of residence time (τ). (a) End of pipe experimental and simulation comparison for τ variation and temperature variation; (b) impact of τ variation on CH_4 conversion and H_2 yield in simulations; (c) Simulation 'C' distribution in product for 1373 K and (d) 1573 K (orange solid bar: C_1, green left side diagonals: C_2, violet right side diagonal:C_6, yellow cross: C_{12}, blue dots: C_{16}, pink small cross: remaining). (For interpretation of the references to colour in this figure legend, the reader is referred to the web version of this article.)

the progress of the reactions.

The simulated end-of-pipe mole fractions for the major species H_2 and CH_4 as well as the hydrocarbon by-products C_2H_4 and C_6H_6 are shown in Fig. 9. For H_2 and CH_4, both the mechanisms produce similar outcomes, as can be seen in Fig. 9 (a), with only minor differences in the trend. In the case of ABF2000, a peak is obtained for the H_2 mole fractions around 1673 K, whereas PolyMech suggests a steady increase instead. In contrast, the simulation results presented in Fig. 9 (b) and Fig. 10 reveal a noticeable difference regarding the formation of by-products. The mole fraction peak for C_2H_4 is observed at lower temperatures for ABF2000 compared to the PolyMech mechanism. Compared to ABF2000, PolyMech predicts a significantly higher C_6H_6 quantity (Fig. 9 (b)), which can be attributed to the C-C coupling reactions that cover larger molecule formation only until C_6H_6. On the contrary, ABF2000 comprises reactions consuming C_6H_6 and the formation of PAHs, i.e. resulting in the peak of C_6H_6 appearing at 1473 K (Fig. 9 (b)) followed by a peak of pyrene appearing at 1623 K (Fig. 10). Notably, the isothermal simulations suggest acetylene (C_2H_2) as the most important by-product reaching up to 10 mol-% of the product distribution at 1873 K (Fig. 10).

Using the same inlet compositions and pressure conditions as in the simulations above, an integral RFA was performed using the ABF2000 mechanism for two temperatures, 1673 K and 1273 K. For 1673 K, the reaction paths of ABF2000 are also compared with those of the PolyMech mechanism. Fig. 11 illustrates the major reaction paths for C-C coupling reactions from the starting molecule CH_4 to C_2H_2. The first step

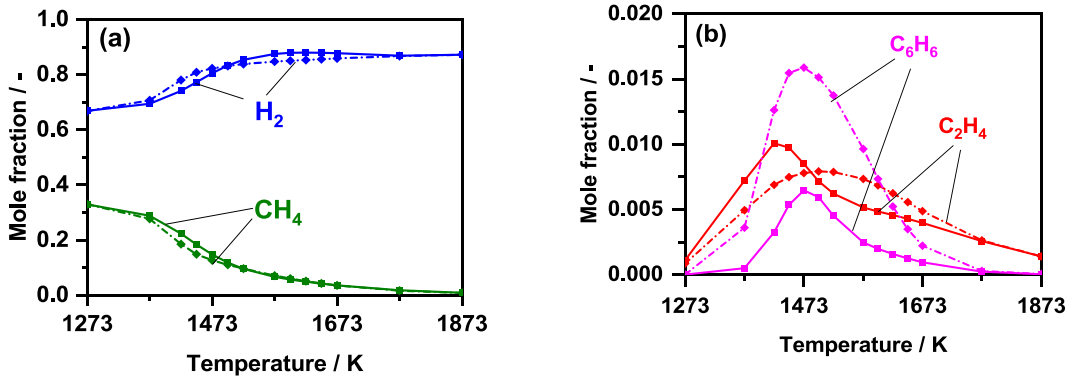

Fig. 9. Simulated end of pipe species mole fractions vs. temperature; (a) Main species, (b) by-products (solid line with (■): ABF2000 mechanism simulation, dot-dashed line with (◆): PolyMech mechanism simulation).

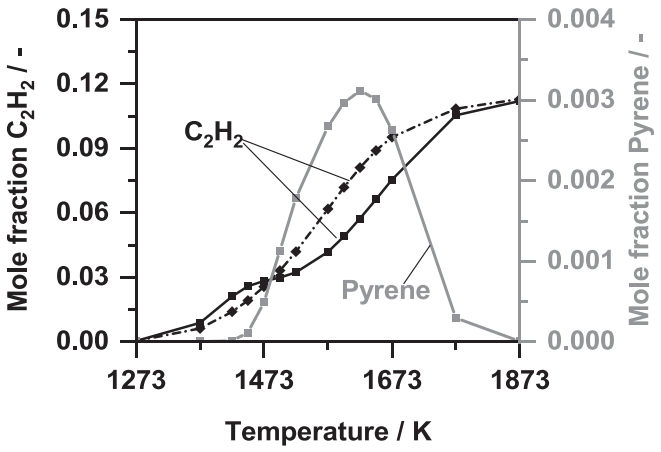

Fig. 10. Simulated end of pipe species mole fractions vs. temperature for by-products that were not detected during the experimental measurements but play a crucial role in simulations (solid line with (■): ABF2000 mechanism, dot-dashed line with (◆): PolyMech mechanism).

in CH_4 pyrolysis is the dissociation of the CH_4 molecule into a CH_3 radical, which is also considered to be the rate determining step in literature [18,35,44,74]. In general, this dissociation can take place via the two reactions given in Equation (10) and (11), which are part of both, ABF2000 and PolyMech. The first reaction describes the direct dissociation via H-atom abstraction by another H-atom, whereas the second reaction represents the dissociation with the help of third body species. At 1673 K, both mechanisms suggest that the direct dissociation is the predominant reaction, which is understandable from a thermodynamic point of view since the high temperatures provide the required energy for bond cleavage. On the contrary, at 1273 K the energy for dissociation is also provided by the third body.

$$CH_4 + M \rightleftharpoons CH_3 + H \tag{11}$$

With regard to C_2 species formation, the coupling of CH_3 radicals into C_2H_6 is the major path in both mechanisms at 1673 K, and a temperature reduction promotes this path even further. From C_2H_4 onwards, C_2H_2 is formed in ABF2000 via an intermediate of C_2H_3, whereas in the case of PolyMech C_2H_2 is directly formed from C_2H_4 by the release of a H_2 molecule. It is interesting to note, that as the C-C coupling reactions proceed, the C to H ratio in the formed hydrocarbons is increasing, since the coupling goes along with dehydrogenation.

From C_2H_2, the onwards reaction pathways till C_6H_6 are shown in Fig. 12 for two temperatures (1273 K and 1673 K) according to the ABF2000 mechanism. Herein, the sub mechanism that describes the formation of aromatic molecules has three pathways. The first is an n-C_4H_3 intermediate path, the second is cyclization reactions of n-C_6H_7 and the third is a recombination of propargyl radicals (C_3H_3). Under reaction conditions typical for CH_4 pyrolysis, the third reaction pathway is dominant. From C_2H_2 onwards, precursors for aromatic molecule formation are produced either via coupling of C_2H_2 with a CH_3 radical to form allene or via propyne formation. These paths strongly depend on the temperature. At 1273 K only allene and propyne are formed from C_2H_2 which subsequently forms C_3H_3, whereas at 1673 K, the formation of i-C_4H_3 is the main path, which leads to the re-formation of C_2H_2 via C_4H_4 and C_4H_2 intermediates.

Modelling the C_3H_3 recombination reaction (Equation (12)) to form the first aromatic ring, i.e. C_6H_6, in a single step is an accepted approach in the literature [40,41,43,75,76].

$$C_3H_3 + C_3H_3 \rightleftharpoons C_6H_6 \tag{12}$$

In both mechanisms, ABF2000 and PolyMech, the reaction is considered to take place in a single step, and is modelled irreversible in ABF2000 on the one hand and reversible in PolyMech on the other hand. In the current work, it is observed that in the case of very high H_2 production the ABF2000 mechanism with its irreversible C_3H_3 recombination reaction does not remain thermodynamically consistent (Fig. S4). Since most of the previous studies performed with this mechanism are combustion-related with smaller residence times, the H_2 production is of comparably minor relevance. A recent study of Chu et al. [67] and an allene pyrolysis study by Kern et al. [75] revealed that pathways leading from propargyl recombination to C_6H_6 formation are in fact not a single step reaction. Appel et al. [41] also mentioned writing C_3H_3 recombination reaction (Equation (12)) as irreversible and in a single step would have a bias towards the experiments considered while developing the mechanism. Therefore, considering this possible reaction sequence is essentially imperative when developing a new CH_4 pyrolysis gas-phase mechanism. However, since the development of a completely new mechanism is beyond the focus of the present study the reaction in ABF2000 is herein written reversible, analogous to the PolyMech mechanism, which ensures thermodynamic consistency even with high levels of H_2 formation.

In the case of PolyMech, the reaction path from C_2H_2 onwards looks slightly different compared to ABF2000 as shown in Fig. 13. Allene and propyne are formed in the first step from C_2H_2. From allene, however, there exists an additional direct reaction path of C_3H_3 and allene reacting to form C_6H_6 formation (Equation (13)).

$$\text{Allene} + C_3H_3 \rightleftharpoons C_6H_6 + H \tag{13}$$

Moreover, from allene onwards, PolyMech includes a path to form propene (C_3H_6) that is not present in ABF2000. Although along with C_3 chemistry also C_4 chemistry plays a crucial role, the latter one does not contribute to the formation of aromatics, but rather results in a closed cycle to re-formation of C_2H_2.

C-C coupling reactions after C_6H_6 are present only in the ABF2000 mechanism. The path of formation of PAHs proceeds according to the HACA reaction sequence. Fig. 14 shows this path for 1673 K, since for lower temperatures PAHs formation is negligible. As a first step, phenyl and an H radical is formed from the C_6H_6 ring. From phenyl onwards, four different paths are established. The reaction path contributing the

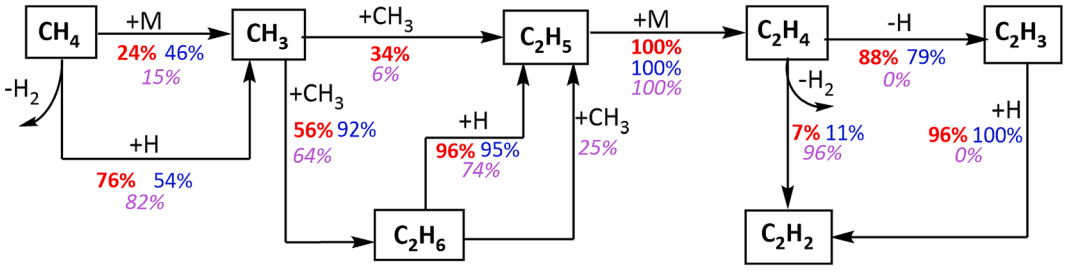

Fig. 11. Integral reaction flow analysis from CH_4 to C_2H_2 formation at 1 bar, H_2:CH_4 molar ratio 2, residence time of 5 s; Red bold number indicate ABF2000 at 1673 K, blue normal font indicates ABF2000 at 1273 K, and violet italic number indicate PolyMech at 1673 K contribution in %). (For interpretation of the references to colour in this figure legend, the reader is referred to the web version of this article.)

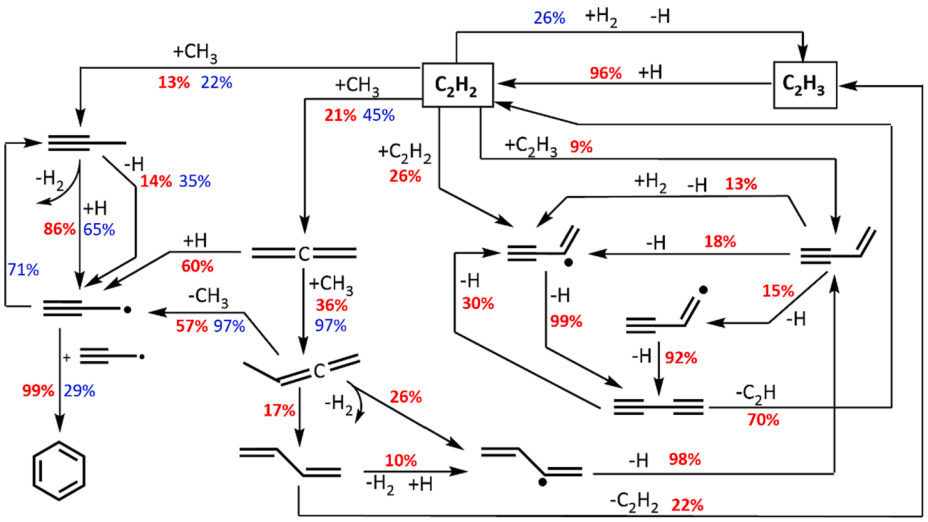

Fig. 12. Integral reaction flow analysis with ABF2000 from C_2H_2 to C_6H_6 formation for 1273 K and 1673 K (pressure of 1 bar, H_2:CH_4 ratio of 2, residence time of 5 s. Red bold numbers indicate a simulation temperature of 1673 K, blue normal font indicates a temperature of 1273 K). (For interpretation of the references to colour in this figure legend, the reader is referred to the web version of this article.)

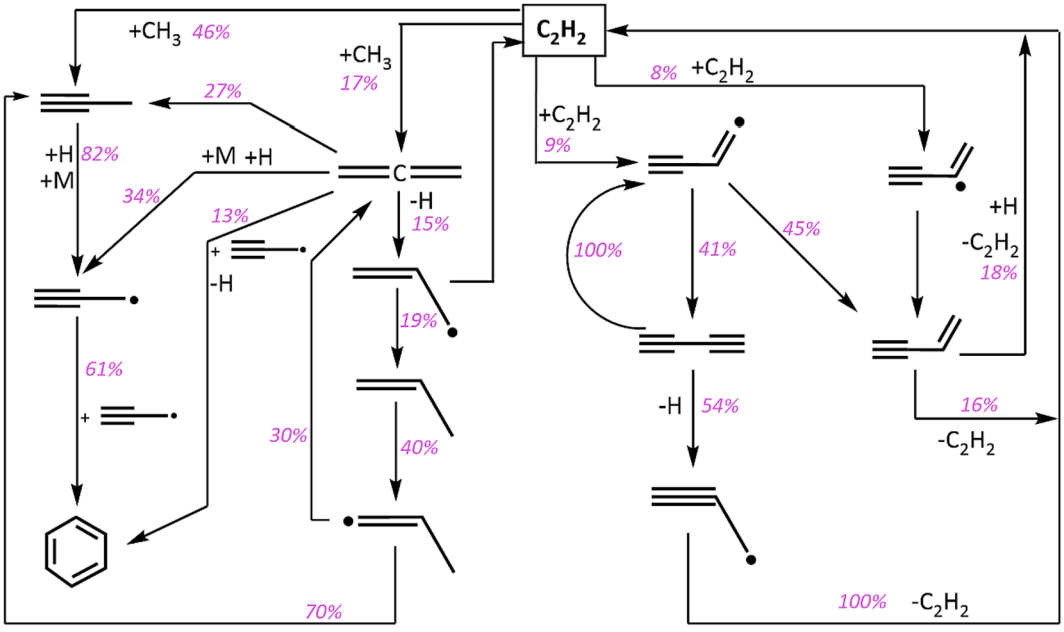

Fig. 13. Integral reaction flow analysis with PolyMech from C_2H_2 to C_6H_6 formation (1673 K, 1 bar, H_2:CH_4 ratio of 2, residence time of 5 s).

least is the one during which the phenyl radical releases an H radical to form benzyne. This is the path where further C_6 rearrangements take place and via C_4 linear hydrocarbons ultimately C_2H_2 is formed back. With a share of 39 %, the major path from benzyne onwards is the addition of C_2H_2 to form phenylacetylene, followed by C_4H_4 addition to form naphthalene (19 %) and C_6H_6 addition to form biphenyl (10 %). These paths see further addition of either C_2H_2 or C_4H_4 to grow the PAHs from the phenanthrene intermediate, until the reaction sequence finally ends forming pyrene and acenaphthylene.

All the RFAs shown in this section point out that C_2H_2 is a central species in CH_4 pyrolysis. Isothermal simulations shown in Fig. 10 also confirm this by predicting C_2H_2 as the main by-product. However, full reactor simulations do not predict a similarly large amount of C_2H_2. Moreover, the axial profile in Fig. 6 (b) shows a drop in C_2H_2 when the cooling zone starts. A RFA is performed with ABF2000, using the gas composition at a position of 0.5 m from the simulation conducted at 1673 K (Fig. 6) as inlet composition. A reduced temperature of 973 K and a residence time of 5 s is specified for RFA, which reveals the direction of the reactions in the cooling zone. The RFA that is displayed in Fig. 15 highlights that 88 % of the C_2H_2 is converted to C_2H_3 and subsequently to C_2H_4 when the temperature is decreased. The reaction also goes further reverse, forming C_2H_6 and CH_4. This explains the trends observed in Fig. 6, namely formation of C_2H_4 and CH_4 in the cooling zone downstream of the isothermal hot zone. It is therefore confirmed, that C_2H_2 is indeed a central by-product also in the case of full reactor simulations. However, the cooling zone at the end of the reactor triggers reverse gas-phase reactions forming C_2H_4, C_2H_6 and CH_4. Additionally, the RFA findings underscore the significance of simulating the entire reactor during CH_4 pyrolysis when a cooling zone is present downstream of the hot reaction zone.

It is important to note that reverse reactions in the context of a flow reactor are complex phenomena. Many parameters influence their

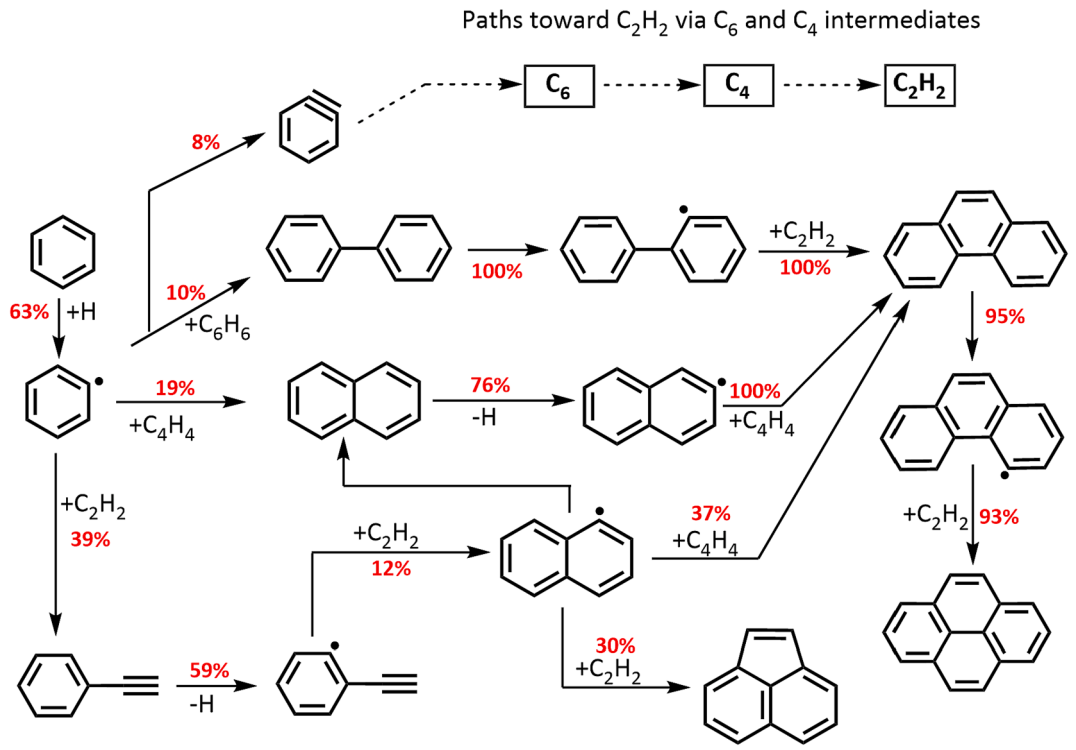

Fig. 14. Integral reaction flow analysis with ABF2000 from C_6H_6 to Pyrene formation (1673 K, 1 bar, H_2:CH_4 ratio of 2, residence time of 5 s).

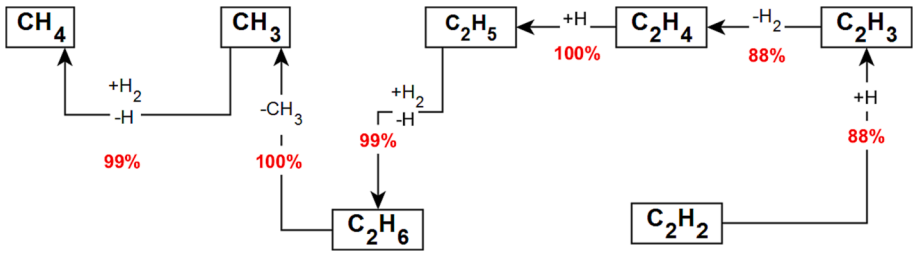

Fig. 15. Integral flow analysis to understand reverse reactions (973 K, 1 bar, composition corresponding to 0.5 m in full reactor simulation in Fig. 6, residence time of 5 s).

occurrence such as the availability of different reactants, temperature and residence time. These reactions occur due to a negative temperature gradient and not due to absolute low temperatures. In fact, below a certain threshold temperature (800 K in case of Fig. 6) these reactions do not take place, which suggests that more reverse reactions will take place in the subsequent cooling zone if the temperature of the hot zone is higher. On the other hand, if hot zone temperatures are higher (>1673 K) and also the hot zone residence time is high enough (>10 s) that the reaction moves forward from C_2H_2 to pyrene, then the impact of reverse reactions would be lower.

In summary, isothermal simulations in combination with an integral reaction flow analysis provide detailed information about the reaction paths evolving along the reactor length or with respect to time. It also explains the possibility of the reverse reactions if a cooling zone is present in the reactor. Furthermore, RFA also identifies important precursors, which will play a crucial role for further work when coupling gas-phase chemistry to surface chemistry such as soot formation or surface deposition.

5. Conclusions

In conclusion, methane pyrolysis gas-phase chemistry was investigated using one-dimensional plug flow reactor simulations with elementary-step-based reaction mechanisms and the results were compared to the experimental data. A thermodynamic analysis was performed to determine the equilibrium limits of CH_4 pyrolysis, considering gas-phase species at a molar H_2:CH_4 ratio of 2 and a pressure of 1 bar. Although the H_2 equilibrium mole fraction reached a peak of 0.9 around 1600 K, the formation of solid carbon during the experiments enabled crossing the gas-phase equilibrium limit, resulting in H_2 mole fractions up to 0.96. Kinetic simulations indicated that temperatures above 1273 K were necessary to initiate CH_4 conversion, which subsequently increased rapidly as the temperature rose to 1573 K. Additionally, the study emphasizes the critical roles of the isothermal hot zone temperature, pre-heating zone upstream, and cooling zone downstream in influencing by-product distribution due to the reverse reactions of light hydrocarbons. Increasing the H_2:CH_4 molar feed ratio led to decreased CH_4 conversion, owing to H_2 inhibition, but also suppressed the formation of polycyclic aromatic hydrocarbons, thereby controlling soot production. Moreover, as residence times increased from 3 s onwards, CH_4 conversion improved only marginally, but the by-product distribution changed due to polycyclic aromatic hydrocarbons formation. The integral reaction flow analysis shed light on reaction paths in the mechanisms ABF2000 and PolyMech, identifying essential precursors for heterogeneous reactions. Simulations exhibited very good agreement with experimental end-of-pipe measurements at

temperatures below 1673 K. However, differences between simulations and experiments at higher temperatures were attributed to heterogeneous reactions taking place during the experiments that are not captured by the corresponding simulations. In future work, elementary-step gas-phase mechanisms will be coupled with heterogeneous soot formation and solid carbon deposition reactions to allow for a holistic description.

Abbreviations

PFR	Plug flow reactor	
List of symbols		
Latin symbols		
c_i	Concentration of gas-phase species i	mol m^{-3}
k_{fk}	Rate of forward reaction	mol m^{-3} s^{-1}
k_{rk}	Rate of reverse reaction	mol m^{-3} s^{-1}
M	Molar mass	kg mol^{-1}
$\dot{n}_{ik}$	Molar rate of species i in reaction k	mol s^{-1}
R_g	Set of gas-phase reactions	-
r_k	Local rate of reaction k	mol m^{-3} s^{-1}
R_k	Total rate of reaction k	mol m^{-3}
S_g	Set of gas-phase species	-
t	Time	s
u	Superficial velocity of gas	m s^{-1}
Y_i	Mass faction of gas-phase species i	-
z	Reactor axial coordinate	m
Greek symbols		
$\Delta_r G$	Gibbs energy of reaction	kg mol^{-1}
ν	Stoichiometric coefficients	-
ρ	Gas mixture density	kg m^{-3}
τ	Residence time	s
$\dot{\omega}_i$	Rate of formation of gas-phase species i	mol m^{-3} s^{-1}

Declaration of competing interest

The authors declare that they have no known competing financial interests or personal relationships that could have appeared to influence the work reported in this paper.

Data availability

Data will be made available on request.

Acknowledgments

We very much appreciate fruitful discussions and experimental support from Corina Janzer (KIT). The authors gratefully acknowledge funding by the Federal Ministry of Education and Research (BMBF) of Germany, project Me^2H_2, grant number 03SF0571B. The omegadot software & consulting GmbH is gratefully acknowledged for a cost-free academic license of DETCHEM.

References

[1] O. Machhammer, A. Bode, W. Hormuth, Financial and Ecological Evaluation of Hydrogen Production Processes on Large Scale, Chem. Eng. Technol. 39 (2016) 1185–1193, https://doi.org/10.1002/ceat.201600023.
[2] N. Sánchez-Bastardo, R. Schlögl, H. Ruland, Methane Pyrolysis for CO_2-Free H_2 Production: A Green Process to Overcome Renewable Energies Unsteadiness, Chem. Ing. Tech. 92 (2020) 1596–1609, https://doi.org/10.1002/cite.202000029.
[3] P. Lott, O. Deutschmann, Heterogeneous chemical reactions-A cornerstone in emission reduction of local pollutants and greenhouse gases, Proc. Combust. Inst. 39 (2023) 3183–3215, https://doi.org/10.1016/j.proci.2022.06.001.
[4] G.A. Olah, A. Goeppert, B. Oil, Beyond Oil and Gas: The Methanol Economy, Wiley-VCH, Weinheim, 2018.
[5] P. Gangadharan, K.C. Kanchi, H.H. Lou, Evaluation of the economic and environmental impact of combining dry reforming with steam reforming of methane, Chem. Eng. Res. Des. 90 (2012) 1956–1968, https://doi.org/10.1016/j.cherd.2012.04.008.
[6] R. Balzarotti, M. Ambrosetti, A. Beretta, G. Groppi, E. Tronconi, Investigation of packed conductive foams as a novel reactor configuration for methane steam reforming, Chem. Eng. J. 391 (2020), 123494, https://doi.org/10.1016/j.cej.2019.123494.
[7] D.P. Serrano, J.A. Botas, J.L.G. Fierro, R. Guil-López, P. Pizarro, G. Gómez, Hydrogen production by methane decomposition: Origin of the catalytic activity of carbon materials, Fuel 89 (2010) 1241–1248, https://doi.org/10.1016/j.fuel.2009.11.030.
[8] L. Weger, A. Abánades, T. Butler, Methane cracking as a bridge technology to the hydrogen economy, Int. J. Hydrogen Energy 42 (2017) 720–731, https://doi.org/10.1016/j.ijhydene.2016.11.029.
[9] U.P.M. Ashik, W.M.A. Wan Daud, H.F. Abbas, Production of greenhouse gas free hydrogen by thermocatalytic decomposition of methane - A review, Renew. Sustain. Energy Rev. 44 (2015) 221–256, https://doi.org/10.1016/j.rser.2014.12.025.
[10] D.A. Hickman, L.D. Schmidt, Production of syngas by direct catalytic oxidation of methane, Science 259 (1993) 343–346, https://doi.org/10.1126/science.259.5093.343.
[11] O. Deutschmann, L. Schmidt, Modeling the partial oxidation of methane in a short-contact-time reactor, AIChE J. 44 (1998) 2465–2477.
[12] R. Schwiedernoch, S. Tischer, C. Correa, O. Deutschmann, Experimental and numerical study on the transient behavior of partial oxidation of methane in a catalytic monolith, Chem. Eng. Sci. 58 (2003) 633–642, https://doi.org/10.1016/S0009-2509(02)00589-4.
[13] M.H. Halabi, M.H.J.M. de Croon, J. van der Schaaf, P.D. Cobden, J.C. Schouten, Modeling and analysis of autothermal reforming of methane to hydrogen in a fixed bed reformer, Chem. Eng. J. 137 (2008) 568–578, https://doi.org/10.1016/j.cej.2007.05.019.
[14] J. Horlyck, C. Lawrey, E.C. Lovell, R. Amal, J. Scott, Elucidating the impact of Ni and Co loading on the selectivity of bimetallic NiCo catalysts for dry reforming of methane, Chem. Eng. J. 352 (2018) 572–580, https://doi.org/10.1016/j.cej.2018.07.009.
[15] A. Giehr, L. Maier, S. Angeli, S.A. Schunk, O. Deutschmann, Dry and Steam Reforming of CH_4 on Co-Hexaaluminate: On the Formation of Metallic Co and Its Influence on Catalyst Activity, Ind. Eng. Chem. Res. 59 (2020) 18790–18797, https://doi.org/10.1021/acs.iecr.0c03522.
[16] S. Hanf, S. Angeli, D. Dussol, C. Fritsch, L. Maier, M. Müller, O. Deutschmann, S. A. Schunk, in: Methane Dry Reforming, Chapter 9 in Chemical Valorisation of Carbon Dioxide, The Royal Society of Chemistry, 2022, pp. 187–207, https://doi.org/10.1039/9781839167645-00187.
[17] O. Schmidt, A. Gambhir, I. Staffell, A. Hawkes, J. Nelson, S. Few, Future cost and performance of water electrolysis: An expert elicitation study, Int. J. Hydrogen Energy 42 (2017) 30470–30492, https://doi.org/10.1016/j.ijhydene.2017.10.045.
[18] N. Sánchez-Bastardo, R. Schlögl, H. Ruland, Methane Pyrolysis for Zero-Emission Hydrogen Production: A Potential Bridge Technology from Fossil Fuels to a Renewable and Sustainable Hydrogen Economy, Ind. Eng. Chem. Res. 60 (2021) 11855–11881, https://doi.org/10.1021/acs.iecr.1c01679.
[19] J.M. Bergthorson, Recyclable metal fuels for clean and compact zero-carbon power, Prog. Energy Combust. Sci. 68 (2018) 169–196, https://doi.org/10.1016/j.pecs.2018.05.001.
[20] C. Kuhn, A. Düll, P. Rohlfs, S. Tischer, M. Börnhorst, O. Deutschmann, Iron as recyclable energy carrier: Feasibility study and kinetic analysis of iron oxide reduction, Appl. Energy Combust. Sci. 12 (2022), 100096, https://doi.org/10.1016/j.jaecs.2022.100096.
[21] A. Düll, P. Rohlfs, O. Deutschmann, M. Börnhorst, Performance Evaluation of KBH_4 as Energy Carrier for Shipping Applications, Chem. Ing. Tech. 94 (2022) 747–759, https://doi.org/10.1002/cite.202100193.
[22] B. Parkinson, M. Tabatabaei, D.C. Upham, B. Ballinger, C. Greig, S. Smart, E. McFarland, Hydrogen production using methane: Techno-economics of decarbonizing fuels and chemicals, Int. J. Hydrogen Energy 43 (2018) 2540–2555, https://doi.org/10.1016/j.ijhydene.2017.12.081.
[23] H.F. Abbas, W.M.A. Wan Daud, Hydrogen production by methane decomposition: A review, Int. J. Hydrogen Energy 35 (2010) 1160–1190, https://doi.org/10.1016/j.ijhydene.2009.11.036.
[24] M. Hadian, K.A. Buist, A.N.R. Bos, J.A.M. Kuipers, Single catalyst particle growth modeling in thermocatalytic decomposition of methane, Chem. Eng. J. 421 (2021), 129759, https://doi.org/10.1016/j.cej.2021.129759.
[25] T. Geißler, A. Abánades, A. Heinzel, K. Mehravaran, G. Müller, R.K. Rathnam, C. Rubbia, D. Salmieri, L. Stoppel, S. Stückrad, A. Weisenburger, H. Wenninger, T. Wetzel, Hydrogen production via methane pyrolysis in a liquid metal bubble column reactor with a packed bed, Chem. Eng. J. 299 (2016) 192–200, https://doi.org/10.1016/j.cej.2016.04.066.
[26] A.A. Munera Parra, D.W. Agar, Molten metal capillary reactor for the high-temperature pyrolysis of methane, Int. J. Hydrogen Energy 42 (2017) 13641–13648, https://doi.org/10.1016/j.ijhydene.2016.12.044.
[27] M. Gautier, V. Rohani, L. Fulcheri, Direct decarbonization of methane by thermal plasma for the production of hydrogen and high value-added carbon black, Int. J. Hydrogen Energy 42 (2017) 28140–28156, https://doi.org/10.1016/j.ijhydene.2017.09.021.
[28] M. Gautier, V. Rohani, L. Fulcheri, J.P. Trelles, Influence of temperature and pressure on carbon black size distribution during allothermal cracking of methane, Aerosol Sci. Technol. 50 (2016) 26–40, https://doi.org/10.1080/02786826.2015.1123214.

[29] A. Indarto, J.W. Choi, H. Lee, H.K. Song, Effect of additive gases on methane conversion using gliding arc discharge, Energy 31 (2006) 2986–2995, https://doi.org/10.1016/j.energy.2005.10.034.

[30] M. Scapinello, E. Delikonstantis, G.D. Stefanidis, The panorama of plasma-assisted non-oxidative methane reforming, Chem. Eng. Process. Process Intensif. 117 (2017) 120–140, https://doi.org/10.1016/j.cep.2017.03.024.

[31] S. Heijkers, M. Aghaei, A. Bogaerts, Plasma-Based CH_4 Conversion into Higher Hydrocarbons and H_2: Modeling to Reveal the Reaction Mechanisms of Different Plasma Sources, J. Phys. Chem. C 124 (2020) 7016–7030, https://doi.org/10.1021/acs.jpcc.0c00082.

[32] A. Magazova, S. Böddeker, N. Bibinov, D.W. Agar, Systematic Simulation Strategy of Plasma Methane Pyrolysis for CO_2-Free H_2, Chem. Ing. Tech. 94 (2022) 690–700, https://doi.org/10.1002/cite.202100181.

[33] S. Kreuznacht, M. Purcel, S. Böddeker, P. Awakowicz, W. Xia, M. Muhler, M. Böke, A. von Keudell, Comparison of the performance of a microwave plasma torch and a gliding arc plasma for hydrogen production via methane pyrolysis, Plasma Process. Polym. (2022), https://doi.org/10.1002/ppap.202200132.

[34] P. Lott, M.B. Mokashi, H. Müller, D.J. Heitlinger, S. Lichtenberg, A.B. Shirsath, C. Janzer, S. Tischer, L. Maier, O. Deutschmann, Hydrogen Production and Carbon Capture by Gas-Phase Methane Pyrolysis: A Feasibility Study, ChemSusChem 16 (2023), e202201720, https://doi.org/10.1002/cssc.202201720.

[35] C. Chen, M.H. Back, R.A. Back, Mechanism of the Thermal Decomposition of Methane, in: L.F. Albright, B.L. Crynes (Eds.), Ind. Lab. Pyrolyses, American Chemical Society, 1976. https://pubs.acs.org/sharingguidelines.

[36] J.M. Roscoe, M.J. Thompson, Thermal Decomposition of Methane: Autocatalysis, Int. J. Chem. Kinet. 17 (1985) 965–990, https://doi.org/10.1016/b978-0-444-82877-4.50028-7.

[37] A.M. Dean, Detailed kinetic modeling of autocatalysis in methane pyrolysis, J. Phys. Chem. 94 (1990) 1432–1439, https://doi.org/10.1021/j100367a043.

[38] F.G. Billaud, F. Baronnet, C.P. Gueret, Thermal Coupling of Methane in a Tubular Flow Reactor: Parametric Study, Ind. Eng. Chem. Res. 32 (1993) 1549–1554, https://doi.org/10.1021/ie00020a003.

[39] A. Holmen, O. Olsvik, O.A. Rokstad, Pyrolysis of natural gas: chemistry and process concepts, Fuel Process. Technol. 42 (1995) 249–267, https://doi.org/10.1016/0378-3820(94)00109-7.

[40] Y. Hidaka, K. Sato, Y. Henmi, H. Tanaka, K. Inami, Shock-tube and modeling study of methane pyrolysis and oxidation, Combust. Flame 118 (1999) 340–358, https://doi.org/10.1016/S0010-2180(99)00010-3.

[41] J. Appel, H. Bockhorn, M. Frenklach, Kinetic modeling of soot formation with detailed chemistry and physics: Laminar premixed flames of C_2 hydrocarbons, Combust. Flame 121 (2000) 122–136, https://doi.org/10.1016/S0010-2180(99)00135-2.

[42] K. Norinaga, V.M. Janardhanan, O. Deutschmann, Detailed Chemical Kinetic Modeling of Pyrolysis of Ethylene, Acetylene, and Propylene at 1073–1373 K with a Plug-Flow Reactor Model, Int. J. Chem. Kinet. 40 (2007) 199–208, https://doi.org/10.1002/kin.20302.

[43] S. Porras, D. Kaczmarek, J. Herzler, S. Drost, M. Werler, T. Kasper, M. Fikri, R. Schießl, B. Atakan, C. Schulz, U. Maas, An experimental and modeling study on the reactivity of extremely fuel-rich methane/dimethyl ether mixtures, Combust. Flame 212 (2020) 107–122, https://doi.org/10.1016/j.combustflame.2019.09.036.

[44] C.-J. Chen, M.H. Back, R.A. Back, The thermal decomposition of methane. II. Secondary reactions, autocatalysis and carbon formation; non-Arrhenius behaviour in the reaction of CH_3 with ethane, Can. J. Chem. 54 (1976) 3175–3184.

[45] A. Holmen, Direct conversion of methane to fuels and chemicals, Catal. Today. 142 (2009) 2–8, https://doi.org/10.1016/j.cattod.2009.01.004.

[46] M.Y. Sinaki, E.A. Matida, F. Hamdullahpur, Development of a reaction mechanism for predicting hydrogen production from homogeneous decomposition of methane, Int. J. Hydrogen Energy 36 (2011) 2936–2944, https://doi.org/10.1016/j.ijhydene.2010.12.002.

[47] J.A. Manion, R.E. Huie, R.D. Levin, D.R. Burgess Jr., V.L. Orkin, W. Tsang, W.S. McGivern, J.W. Hudgens, V.D. Knyazev, D.B. Atkinson, E. Chai, A.M. Tereza, C.-Y. Lin, T.C. Allison, W.G. Mallard, F. Westley, J.T. Herron, R.F. Hampson, D.H. Frizzell, NIST Chemical Kinetics Database, NIST Standard Reference Database 17, Version 7.0 (Web Version), Release 1.6.8, Data version 2015.09, National Institute of Standards and Technology, Gaithersburg, Maryland, (n.d.) 20899–8320. https://kinetics.nist.gov/.

[48] M.H. Back, R.A. Back, Thermal decomposition and reactions of methane, Chapter 1 in Pyrolysis: theory and industrial practice, in: L.F. Albright, B.L. Crynes, W.H. Corcoran (Eds.), Academic Press, 1983: pp. 1–24.

[49] N. Shah, D. Panjala, H. Gerald, Hydrogen production by catalytic decomposition of methane, Energy Fuels 15 (2001) 1528–1534, https://doi.org/10.1016/j.apcatb.2014.02.046.

[50] D.B. Murphy, R.W. Carroll, J.E. Klonowski, Analysis of products of high-temperature pyrolysis of various hydrocarbons, Carbon 35 (1997) 1819–1823, https://doi.org/10.1016/S0008-6223(97)00109-7.

[51] K. Norinaga, O. Deutschmann, K.J. Hüttinger, Analysis of gas phase compounds in chemical vapor deposition of carbon from light hydrocarbons, Carbon 44 (2006) 1790–1800, https://doi.org/10.1016/j.carbon.2005.12.050.

[52] K. Norinaga, O. Deutschmann, Detailed kinetic modeling of gas-phase reactions in the chemical vapor deposition of carbon from light hydrocarbons, Ind. Eng. Chem. Res. 46 (2007) 3547–3557, https://doi.org/10.1021/ie061207p.

[53] S.D. Angeli, S. Gossler, S. Lichtenberg, G. Kass, A.K. Agrawal, M. Valerius, K. P. Kinzel, O. Deutschmann, Reduction of CO_2 Emission from Off-Gases of Steel Industry by Dry Reforming of Methane, Angew. Chemie - Int. Ed. 60 (2021) 11852–11857, https://doi.org/10.1002/anie.202100577.

[54] A. Çelik, I. Ben Othman, H. Müller, P. Lott, O. Deutschmann, Pyrolysis of biogas for carbon capture and carbon dioxide-free production of hydrogen, React. Chem. Eng. (2023), https://doi.org/10.1039/d3re00360d.

[55] O. Deutschmann, S. Tischer, S. Kleditzsch, V. Janardhanan, C. Correa, D. Chatterjee, N. Mladenov, H.D. Minh, H. Karadeniz, M. Hettel, V. Menon, A. Banerjee, H. Gossler, A. Shirsath, E. Daymo, DETCHEM, (2022). http://www.detchem.com.

[56] S. Wan, K. Keller, P. Lott, A.B. Shirsath, S. Tischer, T. Häber, R. Suntz, O. Deutschmann, Experimental and numerical investigation of NO oxidation on Pt/Al_2O_3- and NO_x storage on Pt/ BaO/Al_2O_3-catalysts, Catal. Sci. Technol. 12 (2022) 4456–4470, https://doi.org/10.1039/d2cy00572g.

[57] A.B. Shirsath, M. Mokashi, P. Lott, H. Müller, R. Pashminehazar, T. Sheppard, S. Tischer, L. Maier, J.-D. Grunwaldt, O. Deutschmann, Soot Formation in Methane Pyrolysis Reactor: Modeling Soot Growth and Particle Characterization, J. Phys. Chem. A 127 (2023) 2136–2147, https://doi.org/10.1021/acs.jpca.2c06878.

[58] A.B. Shirsath, M.L. Schulte, B. Kreitz, S. Tischer, J.-D. Grunwaldt, O. Deutschmann, Spatially-resolved investigation of CO_2 methanation over Ni/γ-Al_2O_3 and $Ni_{3.2}Fe$/γ-Al_2O_3 catalysts in a packed-bed reactor, Chem. Eng. J. 469 (2023), 143847, https://doi.org/10.1016/j.cej.2023.143847.

[59] H. Gossler, O. Deutschmann, Numerical optimization and reaction flow analysis of syngas production via partial oxidation of natural gas in internal combustion engines, Int. J. Hydrogen Energy 40 (2015) 11046–11058, https://doi.org/10.1016/j.ijhydene.2015.06.125.

[60] V.I. Golovitchev, F. Tao, J. Chomiak, Numerical evaluation of soot formation control at diesel-like conditions by reducing fuel injection timing, SAE Tech. Pap. (1999), https://doi.org/10.4271/1999-01-3552.

[61] M. Frenklach, H. Wang, M. Goldenberg, G.P. Smith, D.M. Golden, C.T. Bowman, R. K. Hanson, W.C. Gardiner, V. Lissianski, GRI-Mech—an optimized detailed chemical reaction mechanism for methane combustion, Gas Res. Inst. Top. Report, Gas Res. Institute, Chicago. (1995).

[62] A. Roine, HSC Chemistry for Windows, v. 9.4.1 (Pori, Finland: Outotec Research, 2017), (2017). https://www.hsc-chemistry.com/news&tiedoteid=31.

[63] A. Oberlin, Pyrocarbons, Carbon 40 (2002) 7–24, https://doi.org/10.1016/S0008-6223(01)00138-5.

[64] A. Becker, Z. Hu, K.J. Hüttinger, Hydrogen inhibition model of carbon deposition from light hydrocarbons, Fuel 79 (2000) 1573–1580, https://doi.org/10.1016/S0016-2361(00)00030-2.

[65] J. Antes, Z. Hu, W. Zhang, K.J. Hüttinger, Chemistry and kinetics of chemical vapour deposition of pyrocarbon VII. Confirmation of the influence of the substrate surface area/reactor volume ratio, Carbon 37 (1999) 2031–2039, https://doi.org/10.1016/S0008-6223(99)00070-6.

[66] A. Becker, K.J. Hüttinger, Chemistry and kinetics of chemical vapor deposition of pyrocarbon - II pyrocarbon deposition from Ethylene, Acetylene & 1,3-Butadine in the low temperature regime, Carbon 36 (1998) 177–199, https://doi.org/10.1016/S0008-6223(97)00176-0.

[67] T.C. Chu, Z.J. Buras, P. Oßwald, M. Liu, M.J. Goldman, W.H. Green, Modeling of aromatics formation in fuel-rich methane oxy-combustion with an automatically generated pressure-dependent mechanism, Phys. Chem. Chem. Phys. 21 (2019) 813–832, https://doi.org/10.1039/c8cp06097e.

[68] P.A. Tesner, Kinetics of pyrolytic carbon formation, in: P.A. Thrower (Ed.), Chemistry and Physics of Carbon Vol. 19, CRC Press, Boca Raton, 1984.

[69] W. Benzinger, A. Becker, K.J. Hüttinger, Chemistry and kinetics of chemical vapour deposition of pyrocarbon: I. Fundamentals of kinetics and chemical reaction engineering, Carbon 34 (1996) 957–966, https://doi.org/10.1016/0008-6223(96)00010-3.

[70] A. Becker, K.J. Hüttinger, Chemistry and kinetics of chemical vapor deposition of pyrocarbon - III pyrocarbon deposition from propylene and benzene in the low temperature regime, Carbon 36 (1998) 201–211, https://doi.org/10.1016/S0008-6223(97)00176-0.

[71] A. Becker, K.J. Hüttinger, Chemistry and kinetics of chemical vapor deposition of pyrocarbon - IV pyrocarbon deposition from methane in the low temperature regime, Carbon 36 (1998) 213–224, https://doi.org/10.1016/S0008-6223(97)00177-2.

[72] K.J. Hüttinger, CVD in Hot Wall Reactors - The Interaction between Homogeneous Gas-Phase and Heterogeneous Surface Reactions, Chem. Vap. Depos. 4 (1998) 151–158, https://doi.org/10.1002/(sici)1521-3862(199807)04:04<151::aid-cvde151>3.0.co;2-2.

[73] O. Olsvik, O.A. Rokstad, A. Holmen, Pyrolysis of methane in the presence of hydrogen, Chem. Eng. Technol. 18 (1995) 349–358, https://doi.org/10.1002/ceat.270180510.

[74] M. Brüggert, Z. Hu, K.J. Hüttinger, Chemistry and kinetics of chemical vapor deposition of pyrocarbon. VI. Influence of temperature using methane as a carbon source, Carbon 37 (1999) 2021–2030, https://doi.org/10.1016/S0008-6223(99)00069-X.

[75] C.H. Wu, R.D. Kern, Shock-Tube Study of Aliene Pyrolysis, J. Phys. Chem. (1987) 6291–6296, https://doi.org/10.1021/j100308a042.

[76] Y. Hidaka, T. Nakamura, A. Miyauchi, T. Shiraishi, H. Kawano, Thermal decomposition of propyne and allene in shock waves, Int. J. Chem. Kinet. 21 (1989) 643–666, https://doi.org/10.1002/kin.550210805.